Ising model on the Bethe lattice with competing interactions up to the third-nearest-neighbor generation

C. R. da Silva* and S. Coutinho
Departamento de Física, Universidade Federal de Pernambuco, 50 000 Recife, Pernambuco, Brazil
(Received 11 August 1986)

The Ising model on the Bethe lattice of general connectivity, with competing interactions between the first-, second-, and third-neighbor spin generations has been studied. In our approach the partition function, the local magnetization and the pair correlation function are obtained exactly by solving a set of coupled recursion relations of appropriated effective fields. The phase diagram is studied for several ranges of the competing parameters showing the appearance of several features and modulated phases arising from the frustration effects introduced by the third-nearest-neighbor interaction. The ground-state phase diagram is obtained analytically by a minimization procedure and the infinite-connectivity limit is worked out, recovering previous results.

I. INTRODUCTION

The study of exactly solved models deserves some general interest in statistical mechanics.[1] The Ising model on the Bethe lattice with competing interactions is one of these models that has received widespread attention by many authors very recently,[2–7] since the appearance of the Vannimenus model.[2] The Bethe lattice, that is, an infinite connected tree whose sites have the same coordination number, has a thin structure without closed paths but with infinite dimensionality.[1] By introducing competing interactions between $\frac{1}{2}$ Ising spin variables, assigned to each site, we enable the system to present a very rich phase diagram with many modulated phases. The Vannimenus model,[2] that is, the Ising model on a Bethe lattice of coordination number $p=3$, with a ferromagnetic nearest-neighbor interaction and with an antiferromagnetic next-nearest-neighbor interaction (the latter restricted to the sites belonging to the same branch) is the counterpart of the anisotropic next-nearest-neighbor Ising (ANNNI) model defined on regular lattices. In the ANNNI model the competing interactions are restricted to a single direction, while in the Vannimenus model there is no preferential direction at all, that is, the competing interactions act between the ring generations in all directions. The phase diagram of the Vannimenus model shows in addition to the paramagnetic and the ferromagnetic phases a $++--$ periodic antiphase $\langle 2 \rangle$ and a modulated phase, all of which meet at a multicritical point at zero temperature.[2] If next-nearest-neighbor interbranch interactions are allowed, that is, interactions between sites belonging to the same generation, frustration effects are much more prominent than those in the Vannimenus model since closed loops have been introduced within the lattice. Inawashiro, Thompson, and Honda[4] considered this later case finding that the modulated phase actually consists of small region of commensurated phases interspersed in a chaotic phase. They found also that the chaotic phase persists over a finite range of values of the competing parameter even at zero temperature. Mariz, Tsallis, and Albuquerque[6] extended this model to the general case where the interbranch competing interaction has a different coupling constant from the intrabranch interactions, showing that the modulated phase is stable for a finite range of values of the competing parameter. Yokoi, Oliveira, and Salinas[7] studied the Vannimenus model in the infinite coordination number limit. They found within this limit a phase diagram much richer than the Vannimenus diagram displaying, in addition to the modulated phases, a Lifshitz point. They also found strong numerical evidence for the existence of a complete devil's staircase at low temperatures and of chaotic phases associated with strange attractors. Frustration effects due to the competition between the exchange interaction and the applied external field has been considered by Morita,[8] and Horiguchi and Morita,[5] who studied a regular Ising model with nearest-neighbor interactions of J and $-J$ ($J>0$) on a Cayley tree of coordination number three. In their model, for each site there are two ferromagnetic interactions $+J$ and one antiferromagnetic interaction $-J$ and the phase diagram shows the existence of a spin-glass and a spin-crystal phase besides the paramagnetic one.

In this paper we studied the Ising model on a general Bethe lattice with arbitrary coordination number and with competing interactions between the first-, second-, and third-next-nearest-neighbor spins belonging to the same branch, and in the presence of an external magnetic field. The extension of the ANNNI model to include third-nearest-neighbor interactions (A3NNI model) has been proposed by Yamada and Hamaya[9] in an attempt to explain the phase diagram structure of several ferroelectric systems of the type A_2BX_4. In these materials the wide variety of lock-in phases is attributed to the existence of different stable modulated phases in the ground state. The inclusion of the third-nearest-neighbor competing interaction is essential for the presence of these phases at $T=0$ as will be shown later in the present paper. Very recently[10–12] the A3NNI model has been studied in the framework of low-temperature series technique[10,11] and under the presence of a uniform external field within the mean-field approximation.[12]

In the present paper we have generalized the approach

used by Thompson[13] for the Ising model on the Bethe lattice with only nearest-neighbor interactions and an external field. We were able to calculate exactly the partition function, the local magnetization, and the pair correlation function, by solving numerically a system of high-order coupled recursion equations for partial effective fields. We note that our approach is particularly appropriated for calculating the pair correlation functions. If we neglect the third-nearest-neighbor interaction for zero field we recover the Vannimenus results,[2] and by considering only nearest-neighbor interaction and external field the Thompson results[13] are obtained as expected.

The phase diagrams of our model can be obtained by studying the behavior of local magnetization and of the pair correlation function versus the generation number, and by looking at the fixed points of the coupled recursion relations for the partial effective fields. These diagrams have particularly distinct features depending on the range of competing parameters. If the first- and third-nearest neighbors are coupled ferromagnetically and the second-nearest neighbors antiferromagnetically, the phase diagram has a multicritical point at nonzero temperature where the ferromagnetic, paramagnetic, modulated, and the antiphase $\langle 2 \rangle$ met. If the first-nearest neighbors are coupled ferromagnetically and the second and third are coupled antiferromagnetically, the phase diagram appears to have a quite different form. In this latter case, where the frustration effects are more prominent, we note the appearance of a periodic $++\!+\!---$ antiphase $\langle 3 \rangle$ in addition to the previous ones, and the existence of two multicritical points at zero temperature. It is also observed an enhancement of the modulated region due to the increasing of the frustration effects.

We have also studied the ground-state phase diagram showing that a finite number (four) of lower-order commensurate phases are stable unlike in the ANNNI models because of the introduction of the third-nearest-neighbor competing interaction as expected.[11] Finally, we work out the infinite coordination number limit recovering previous results.[7,14]

This paper has been organized in the following way. In Sec. II the model Hamiltonian is discussed and the approach to obtain the recursion for the partial effective fields is defined. The calculations for the local properties (local magnetization and pair correlation functions) are also presented in this section. Section III is devoted to the discussion of the phase diagram features. The infinite coordination number limit is shown in Sec. IV and finally, the conclusions are given in Sec. V.

II. THE MODEL HAMILTONIAN: THE EFFECTIVE FIELDS, THE PARTITION FUNCTION, AND THE LOCAL PROPERTIES

A. Partition function

We construct the general Bethe lattice of coordination number $p=q+1$ (q is the connectivity number) with $N+1$ generation shells by connecting to a central site (zeroth generation) p sites in order to constitute the first generation. The successive generations can be equally constructed by connecting q sites to each site of the previous generation until we reach the Nth generation. We define our model by considering that each site of the Bethe lattice is assigned with a $\frac{1}{2}$ spin variable which is coupled by exchange interactions with its nearest neighbors (coupling constant J_1), second-nearest neighbors (coupling constant J_2), and third-nearest-neighbors (coupling constant J_3). The second- and the third-nearest-neighbors interactions are allowed only between sites belonging to the same branch, that is, between sites belonging to the second- and to the third-nearest-neighbor generations, respectively. In Fig. 1 we show a particular case of a Bethe lattice with $N=3$ and $p=3$ sketching the exchange interaction in one of the branches. An external uniform field H is considered to act on each site.

The Hamiltonian for this model can be written as

$$\mathscr{H}=-J_1\sum_{n=0}^{N}\sigma_n\sigma_{n+1}-J_2\sum_{n=0}^{N-1}{}'\sigma_n\sigma_{n+2} -J_3\sum_{n=0}^{N-2}{}'\sigma_n\sigma_{n+3}+H\sum_i\sigma_i\ , \tag{2.1}$$

where n labels the generation shells. The first summation involves all pairs of nearest-neighbor sites belonging to two consecutive shells while the second and the third summations are restricted to pairs of sites belonging to the same branch as explained above. The summation over the field is extended to all sites of the lattice.

The exact partition function $Z_{N+1}=\mathrm{Tr}\exp(-\beta H)$ can be written as

$$Z_{N+1}=\sum_{\sigma_0}Z_{N+1}^{\sigma_0}=Z_{N+1}^{+}+Z_{N+1}^{-}\ , \tag{2.2}$$

where $Z_{N+1}^{\sigma_0}$ is the partial partition function where the central site has a $\sigma_0=\pm 1$ defined value. We can write $Z_{N+1}^{\sigma_0}$ in terms of the partition functions of connected branches with $(N+1)$ generations as shown schematically in Fig. 2, that is

$$Z_{N+1}^{\sigma_0}=e^{-Bq\sigma_0}\left[\sum_{\sigma_1}f(\sigma_0,\sigma_1)\left[\sum_{\sigma_2}Z_{N+1}(\sigma_0,\sigma_1,\sigma_2)\right]^q\right]^p\ , \tag{2.3}$$

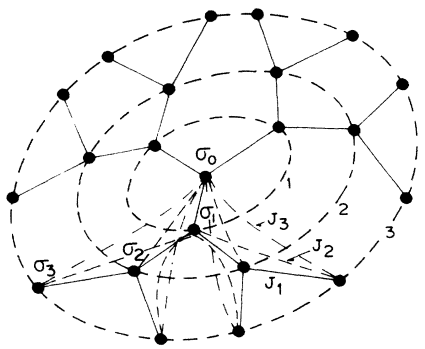

FIG. 1. Bethe lattice with $p=3$ and $N=3$ with the first- (——), and second- (— — —), and third- (—·—·—·) nearest-neighbor interactions sketched in one branch.

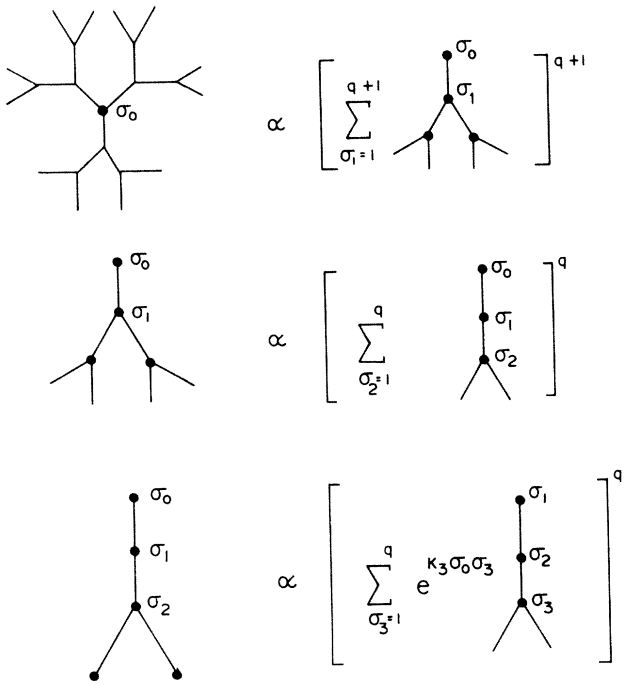

FIG. 2. Schematic way of pruning the lattice branches for writing the partition function $Z_{N+1}^{\sigma_0}$ in terms of the partial partition functions $Z_{N+1}(\sigma_0,\sigma_1,\sigma_2)$.

where

$$Z_{N+1}(\sigma_0,\sigma_1,\sigma_2)=g(\sigma_0,\sigma_1,\sigma_2)f(\sigma_1,\sigma_2)\times\left[\sum_{\sigma_3}e^{K_3\sigma_0\sigma_3}Z_N(\sigma_1,\sigma_2,\sigma_3)\right]^q , \tag{2.4}$$

$$f(\sigma,\sigma')=\exp\{-(q-1)[K_1\sigma\sigma'+B(\sigma+\sigma')]\} , \tag{2.5}$$

$$g(\sigma,\sigma',\sigma'')=\exp(B\sigma+K_1\sigma\sigma'+K_2\sigma\sigma'') , \tag{2.6}$$

and where $B=\beta H$, $K_\alpha=\beta J_\alpha$ ($\alpha=1,2,3$), β being $(k_BT)^{-1}$ as usual. We notice that the $f(\sigma,\sigma')$ is introduced to prevent counting once more the energy factors. We note that by using the recursion relation given by Eq. (2.4) we find that the partition function of the $N+1$ generation lattice can be written by means of the partition functions of branches with N generations. It can be seen later that this process of decimating the lattice by pruning this type of branch is particularly useful for calculating the local properties.

B. Effective fields

The eight recursion relations given by Eq. (2.4) by assuming σ_0, σ_1, and $\sigma_2=\pm1$ can be reduced to four equivalent relations in terms of appropriated effective fields defined as follows:

$$\exp(2a_{n+1})=\frac{Z_{N+1}(+++)}{Z_{N+1}(++-)} , \tag{2.7a}$$

$$\exp(2b_{n+1})=\frac{Z_{N+1}(+-+)}{Z_{N+1}(+--)} , \tag{2.7b}$$

$$\exp(2c_{n+1})=\frac{Z_{N+1}(-++)}{Z_{N+1}(-+-)} , \tag{2.7c}$$

$$\exp(2d_{n+1})=\frac{Z_{N+1}(--+)}{Z_{N+1}(---)} . \tag{2.7d}$$

By substituting Eq. (2.4) in Eqs. (2.7) we can get, after a straightforward calculation, the following coupled recursion relations for the effective fields:

$$a_{n+1}=B+K_1(1-q)+K_2(1-q^2)+q^3A_3(d_{n-2})+q^2B_3^+(b_{n-1},d_{n-1})+qB_3^+(a_n,b_n) , \tag{2.8a}$$

$$b_{n+1}=B-K_1(1+q)+K_2(1-q^2)+q^3A_3(d_{n-2})+q^2B_3^-(b_{n-1},d_{n-1})+qB_3^+(c_n,d_n) , \tag{2.8b}$$

$$c_{n+1}=B+K_1(1-q)-K_2(1+q^2)+q^3A_3(d_{n-2})+q^2B_3^+(b_{n-1},d_{n-1})+qB_3^-(a_n,b_n) , \tag{2.8c}$$

$$d_{n+1}=B-K_1(1+q)-K_1(1+q^2)+q^3A_3(d_{n-2})+q^2B_3^-(b_{n-1},d_{n-1})+qB_3^-(c_n,d_n) , \tag{2.8d}$$

where

$$A_\alpha(x)=\tanh^{-1}(\tanh K_\alpha\tanh x) , \tag{2.9}$$

$$B_\alpha^\pm(x,y)=\tfrac{1}{2}\ln(e^{\pm2K_\alpha+2x}+1)/(e^{\pm2K_\alpha+2y}+1) , \tag{2.10}$$

α being equal to 1, 2, or 3.

The recursion relations given by Eqs. (2.8) constitute a system of four third-order maps that, due to their symmetry, can be reduced to

$$d_{n+1}=B-K_1(1+q)-K_2(1+q^2)+q^3A_3(d_{n-2})+q^2B_3^-(g_{n-1}+d_{n-1}+2K_2,d_{n-1})+qB_3^-(e_n+d_n,d_n) , \tag{2.11a}$$

$$e_{n+1}=2K_1+q^2A_3(g_{n-1}+d_{n-1}+2K_2)-q^2A_3(d_{n-1})+qB_3^-(e_n+f_n+d_n+2K_2,g_n+d_n+2K_2)-qB_3^-(e_n+d_n,d_n) , \tag{2.11b}$$

$$f_{n+1}=qA_3(e_n+f_n+d_n+2K_2)-qA_3(g_n+d_n+2K_2) , \tag{2.11c}$$

$$g_{n+1}=qA_3(e_n+d_n)-qA_3(d_n) , \tag{2.11d}$$

where we have defined the new variables by

$$e_n=c_n-d_n , \tag{2.12a}$$

$$f_n=a_n-c_n-2K_2 , \tag{2.12b}$$

$$g_n=b_n-d_n-2K_2 . \tag{2.12c}$$

Now the system of coupled recursion relations is reduced to one third-order, one second-order and two first-order maps.

As it will be seen later, the local properties (magnetization and pair correlation function) will be calculated in terms of the fixed points or attractors of the recursion relations of the effective fields. Therefore, the reduction of the order of the equations is very important for the numerical calculations.

In the absence of the third-nearest-neighbor interactions ($J_3=0$) we have $A_3(x_n)=0$ and $f_n=g_n=0$, $n=1,\ldots$. Therefore the system of recursion relations is reduced to

$$e_{n+1}=2K_1+qA_2(e_n+d_n+K_2)-qA_2(d_n+K_2)\ , \tag{2.13a}$$

$$h_{n+1}=B-K_1(1+q)+q^2A_2(d_{n-1}+K_2)+qB_2^-(e_n+h_n,h_n)\ , \tag{2.13b}$$

where $h_n=d_n+k_2$.

Equations (2.13) represent the system of coupled recursion relations for the two effective fields for the Vannimenus model for arbitrary coordination number and under an external field. The local magnetization and the pair correlation function of the Vannimenus model can be evaluated exactly from the fixed points or attractors of these coupled maps and its phase diagram can be also obtained.

If we go further by neglecting the second-nearest-neighbor exchange interactions ($J_2=0$) we have $A_2(x_n)=0$, $h_n=d_n$ and the system reduces to one first-order equation, that is

$$l_{n+1}=B+q\tanh^{-1}(\tanh K_1\tanh l_n)\ , \tag{2.14}$$

which is the recursion equation for the effective field of the Ising model on a Bethe lattice with nearest-neighbor exchange interactions only and an external field.[15]

C. Local properties: local magnetization and pair correlation function

In order to investigate the phase diagram of our model we have to look at the local properties, that is, the local magnetization or the magnetization of the central site and the pair correlation function between sites deeply in the interior of the lattice. Perruggi[16] has clarified the dichotomy between the clashing alternative approaches for investigating one-step Markov-Hamiltonian models on Bethe lattices. He emphasizes that the so-called Cayley tree solution, that is, the use of the thermodynamic limit of the free energy for calculating extensive properties like the magnetization, generate results not related to the system, since it takes into account the non-negligible surface effects which arise in the process. We remind the reader that the ratio for the number of surface sites to the total number of sites of the Bethe lattice is $(q-1)$ in the thermodynamic limit. On the other hand, the approaches where the partition function of finite system is used to calculate local properties, and subsequently the thermodynamic limit is taken, gave exact results although they may be criticized from the formal point of view.[15] We believe that Peruggi's conclusions also hold for our three-step Markov model although it has not been proved.

We define the magnetization of the central site by

$$\langle\sigma_0\rangle=\lim_{H\to 0}\lim_{N\to\infty}\frac{1}{Z_{N+1}}\mathrm{Tr}(\sigma_0 e^{-\beta H})=\lim_{H\to 0}\lim_{N\to\infty}\frac{(Z_{N+1}^+/Z_{N+1}^-)-1}{(Z_{N+1}^+/Z_{N+1}^-)+1}\ . \tag{2.15}$$

We can evaluate the ratio (Z_{N+1}^+/Z_{N+1}^-) in terms of the effective fields by using Eqs. (2.3) and (2.4), and the definitions of the effective fields given by Eqs. (2.7). We get, after straightforward calculations,

$$\frac{Z_{n+1}^+}{Z_{n+1}^-}=\exp\{2[-K_1-qK_2+C_3(d_n)+q^2A_3(d_n)]\}\times\left[\frac{\exp\{2[K_1+C_3(d_{n-1})+q^2B_3^+(b_n,d_n)]\}D(a_{n+1})+D(b_{n+1})}{\exp\{2[-K_1+C_3(d_{n-1})+q^2B_3^-(b_n,d_n)]\}D(c_{n+1})+D(d_{n+1})}\right]^{q+1}\ , \tag{2.16}$$

where

$$C_\alpha(x)=B-qK_1-q^2K_2+q^3A_\alpha(x)\ , \tag{2.17}$$

$$D(x)=(e^{2x}+1)^q\ . \tag{2.18}$$

$A_\alpha(x)$ and $B_\alpha^\pm(x,y)$ are given by Eqs. (2.9) and (2.10), respectively. The pair correlation function $\langle\sigma_0,\sigma_1\rangle$ is defined as usual, that is,

$$\langle\sigma_0,\sigma_1\rangle=\lim_{H\to 0}\lim_{N\to\infty}\frac{1}{Z_{N+1}}\sum_{\{\sigma\}}\sigma_0\sigma_1\exp(-\beta H)\ . \tag{2.19}$$

By using the Eqs. (2.3) and (2.4) we can write

$$\langle\sigma_0\sigma_1\rangle=\lim_{H\to 0}\lim_{n\to\infty}\left\{\sum_{\sigma_0}\sigma_0 e^{-Bq\sigma_0}\left[\sum_{\sigma_1}\sigma_1 f(\sigma_0,\sigma_1)\left[\sum_{\sigma_2}Z_{N+1}(\sigma_0,\sigma_1,\sigma_2)\right]^q\right]\times\left[\sum_{\sigma_1}f(\sigma_0,\sigma_1)\left[\sum_{\sigma_2}Z_{N+1}(\sigma_0,\sigma_1,\sigma_2)\right]^q\right]^q\right\}\times\left\{\sum_{\sigma_0}e^{-Bq\sigma_0}\left[\sum_{\sigma_1}f(\sigma_0,\sigma_1)\left[\sum_{\sigma_2}Z_{N+1}(\sigma_0,\sigma_1,\sigma_2)\right]^q\right]^{q+1}\right\}^{-1}\ , \tag{2.20}$$

TABLE I. Sequences of stable fixed points of the recursion relations that characterizes each phase.

Phase	Sequence
Paramagnetic	One fixed point with $a^* \neq -d^*$, $b^* = -c^*$, $a^* \neq b^*$
Ferromagnetic (+ + + + + + + + + . . .)	One fixed point with $a^* \neq b^* \neq c^* \neq d^*$
Antiphase ⟨2,2⟩ (+ + − − + + − − + + . . .)	Four fixed points with $a_i^* = a_{i+4}^* = -d_{i+2}^*$, $b_i^* = b_{i+4}^* = c_{i+2}^*$, $a_i^* \neq b_i^*$
Antiphase ⟨3,3⟩ (+ + + − − − + + + − − − + + + . . .)	Six fixed points with $a_i^* = a_{i+6}^* = -d_{i+3}^*$, $b_i^* = b_{i+6}^* = -c_{i+3}^*$, $a_i^* \neq b_i^*$
Antiphase ⟨2,1⟩ (+ + − + + − + + − . . .)	Three fixed points with $a_i^* = a_{i+3}^*$, $b_i^* = b_{i+3}^*$, $c_i^* = c_{i+3}^*$, $d_i^* = d_{i+3}^*$, $a^* \neq b^* \neq c^* \neq d^*$
Antiferromagnetic ⟨1,1⟩ (+ − + − + − + − + . . .)	Two fixed points with $a_i^* = a_{i+2}^* = -d_{i+1}^*$, $b_i^* = b_{i+2}^* = -c_{i+1}^*$, $a^* \neq b^*$
Modulated	High sequences of fixed points or attractors

where $f(\sigma,\sigma')$ is given by Eq. (2.5). Now, if we make use again of the effective fields definition, given by the Eqs. (2.7), we get after straightforward calculations that

$$\langle \sigma_0 \sigma_1 \rangle = \lim_{n \to \infty} \frac{E_n^2[F_n^+ D(a_{n+1}) - D(b_{n+1})][F_n^+ D(a_{n+1}) + D(b_{n+1})]^q - [F_n^- D(c_{n+1}) - D(d_{n+1})][F_n^- D(c_{n+1}) + D(d_{n+1})]^q}{E_n^2[F_n^+ D(a_{n+1}) + D(b_{n+1})]^{q+1} + [F_n^- D(c_{n+1}) + D(d_{n+1})]^{q+1}} , \tag{2.21}$$

where

$$E_n = \exp[-K_1 - qK_2 + C_3(d_n) + q^2 A_3(d_n)] , \tag{2.22}$$

$$F_n^{\pm} = \exp\{2[\pm K_1 + C_3(d_n) + q^2 B_3^{\pm}(b_n, d_n)]\} . \tag{2.23}$$

Now, with the solutions of the Eqs. (2.15), (2.16), and (2.21) we can study the phase diagram of the model.

III. THE PHASE DIAGRAM

In this section, we present a qualitative study of the exact phase diagram of our model in the (t,α,δ) space for a fixed q, where $t = k_B T/J$ is the reduced temperature, $\alpha = -J_2/J_1$ and $\delta = -J_3/J_1$ are the competing parameters. This can be achieved numerically by observing the qualitative behavior and evolution of fixed points of the

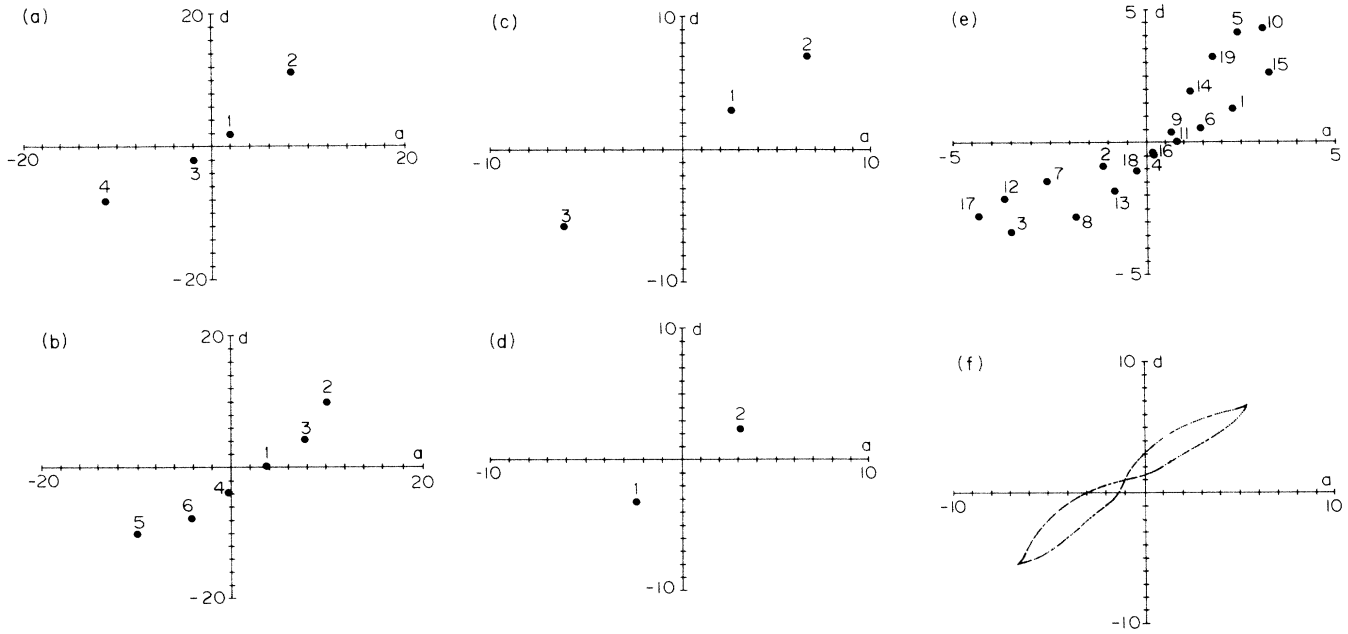

FIG. 3. Fixed points in the (a^*,d^*) plane for the phases (a) antiphase ⟨2,2⟩, (b) antiphase ⟨3,3⟩, (c) antiphase ⟨2,1⟩, (d) antiferromagnetic, (e) high-order commensurate, and (f) incommensurate.

recursion relations given by Eqs. (2.11) after a large number of iterations steps or/and by evaluating the local magnetization and the pair correlation function given by Eqs. (2.15) and (2.21), respectively. In order to obtain the correct thermodynamic limit result we must start with $H \neq 0$ (at least for the spins in the surface shell) before running the iteration calculations, since the $H \to 0$ limit should, therefore, only be taken after the thermodynamic limit (infinite step iterations). Nevertheless, for numerical purposes this procedure is equivalent to taking some very small but finite value of H in the recursion relations.

The phases are characterized by sequences of stable fixed points of the recursions relations in the effective fields space. In Table I these relations are presented.

In Figs. 3(a)—3(f) we show examples of the fixed points in the (a,d) plane for typical points of the modulated

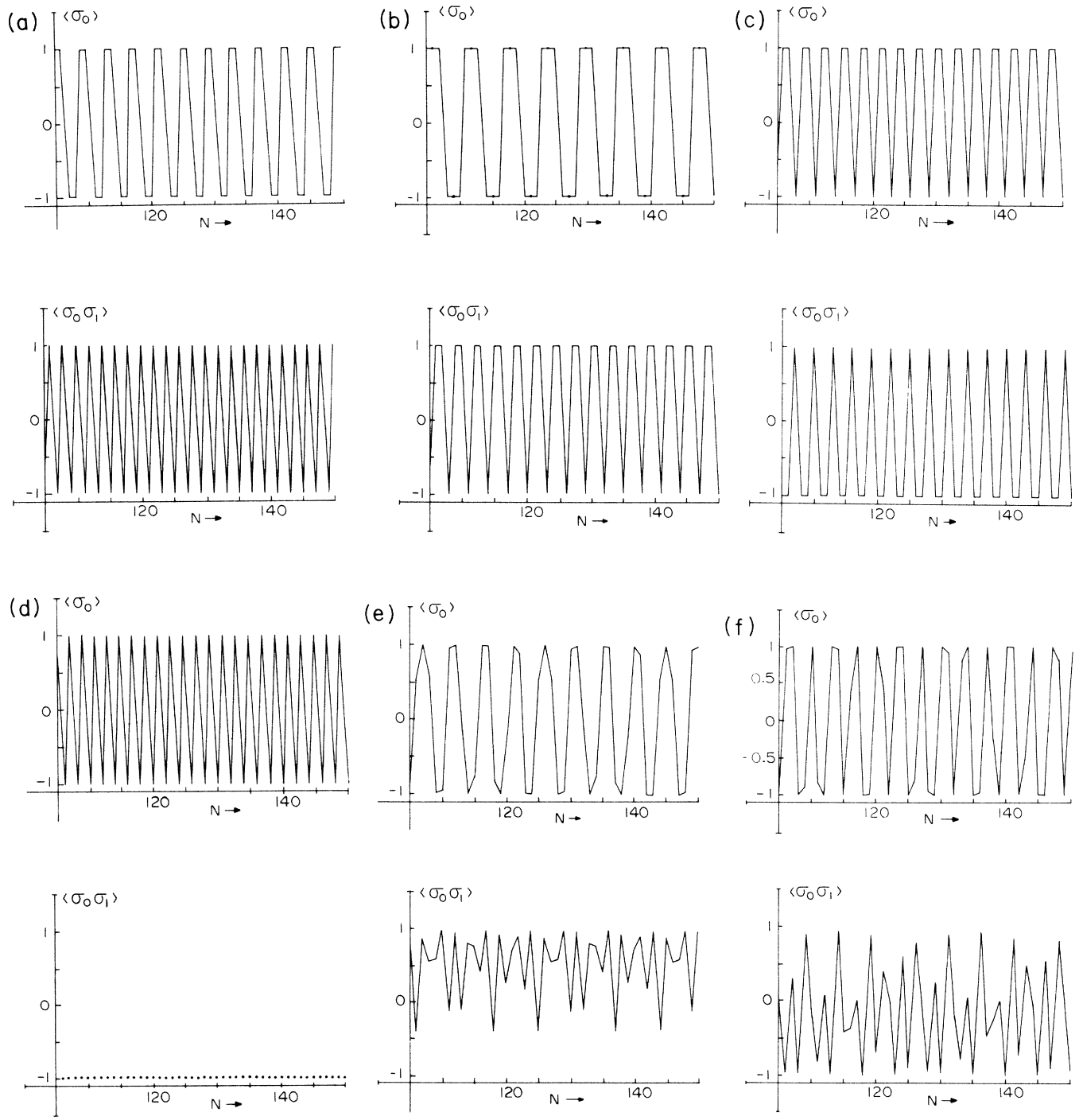

FIG. 4. Local magnetization and pair correlation function versus the generation number in the phases (a) antiphase ⟨2,2⟩, (b) antiphase ⟨3,3⟩, (c) antiphase ⟨2,1⟩, (d) antiferromagnetic, (e) high-order commensurate, and (f) incommensurate.

phases in the (t,α,δ,q) space. The ferromagnetic phase (F) is identified by one single stable fixed point, obtained for $\alpha<0$ and $\delta<0$, at low temperature. In this point we should have $\langle\sigma_0\rangle\neq 0$ and $\langle\sigma_0\sigma_1\rangle=1$. If the temperature is raised the ferromagnetic fixed point evolves continuously to a fixed point lying along the $a=-d$ line. In this case the local magnetization vanishes $\langle\sigma_0\rangle=0$ as well as the pair correlation function $\langle\sigma_0\sigma_1\rangle$ characterizing the paramagnetic phase (P). The ground-state modulated phase $\langle 1,1\rangle$ (antiferromagnetic), $\langle 2,1\rangle$, $\langle 2,2\rangle$, and $\langle 3,3\rangle$ are characterized by sequences of two, three, four, and six fixed points as shown in Figs. 3(a)–3(d). The lower-order commensurate phases (short period) are described by a sequence of a few fixed points while the higher-order commensurate phase (large period) or incommensurate phases (infinite period) are described by quasicontinuous or continuous attractors as shown in Figs. 3(e) and 3(f), respectively.[17]

The phases can also be described by the local magnetization $\langle\sigma_0\rangle$ and the pair correlation function $\langle\sigma_0\sigma_1\rangle$. We can plot both quantities against the shell label n after a large number of iterations. This plot should represent the shell magnetization and the pair correlation function deeply in the interior of the tree. In Figs. 4(a)–4(f) we show the local magnetization and the pair correlation function evaluated at the same points, in the (t,α,δ,q) space as used in Figs. 3(a)–3(f), respectively.

To obtain the phase diagrams, firstly, we assume that $q=2$ and $J_1>0$ and look at the phase diagram in the plane (α,t) for δ fixed. For $-2/(1+q^2)<\delta<0$ ($J_3>0$) we get a typical diagram, as shown in Fig. 5, where the main feature is the existence of a multiphase point at finite temperature where the paramagnetic (P), ferromagnetic (F), antiphase $\langle 2,2\rangle$ and modulated (M) phases met. This diagram is quite similar to the one obtained by Vannimenus.[2] The latter can be easily reproduced if we do have $\delta=0$ showing that the multiphase point drops to the point $T=0$, $\alpha=1/(1+q)$. For $\delta<-2/(1+q^2)$ the phase diagram, shown in Fig. 6, is quite different from the previous one. For $\alpha>(1+q)/(1+q^2)$ we note the appearance of the antiphase $\langle 2,1\rangle$, reflecting the frustration

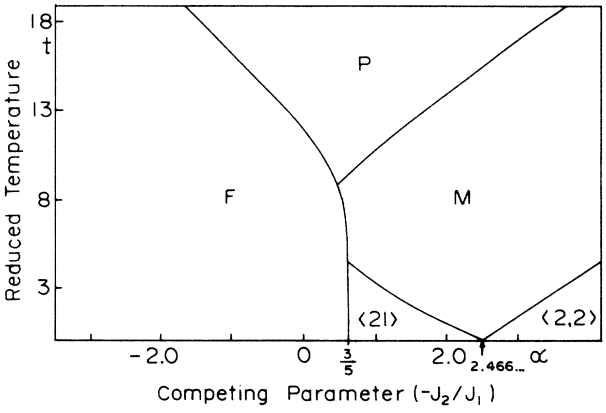

FIG. 6. Phase diagram in the (α,t) plane for $q=2$ and $\delta=-1.2$.

effects arising from the competition between the second-nearest-neighbor antiferromagnetic interaction and the third-nearest-neighbor ferromagnetic interaction.

The phase diagrams for $\delta>0$, that is when the second- and the third-nearest-neighbor interactions are both antiferromagnetic, have also two distinct regions to be analyzed. For $0<\delta<1$ we have the diagram shown in Fig. 7, where we note the presence of the antiphase $\langle 3,3\rangle$ in addition to the F, P, $\langle 2,2\rangle$, and M phases. We also note that the $\langle 3,3\rangle$ phase is symmetric about the point $\alpha=1/(q+1)$ and reaches the P phase dividing the M phase in two regions. Nevertheless for $\delta>1$ the antiferromagnetic (AF) is stable against the ferromagnetic phase due to the large strength of the third-nearest-neighbor antiferromagnetic interaction, as shown in Fig. 8. It can seem in this diagram that the AF phase is reentrant into the whole diagram. We pointed out that the multiphase point $t=0,\alpha=-q$ is independent of δ. Now, we can look at the phase diagrams in the (δ,t) plane. We draw our attention to the $\alpha<-q$ region where there is a coex-

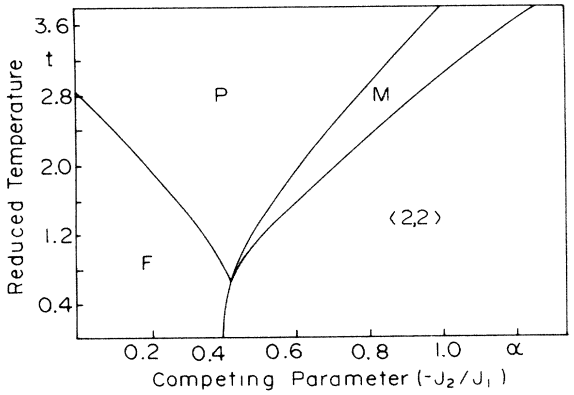

FIG. 5. Phase diagram in the (α,t) plane for $q=2$ and $\delta=-0.1$.

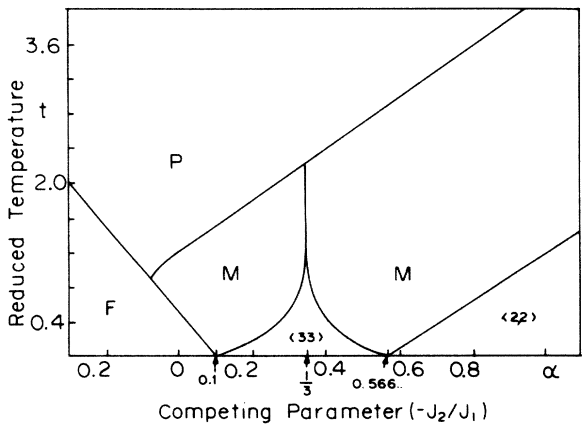

FIG. 7. Phase diagram in the (α,t) plane for $q=2$ and $\delta=0.1$.

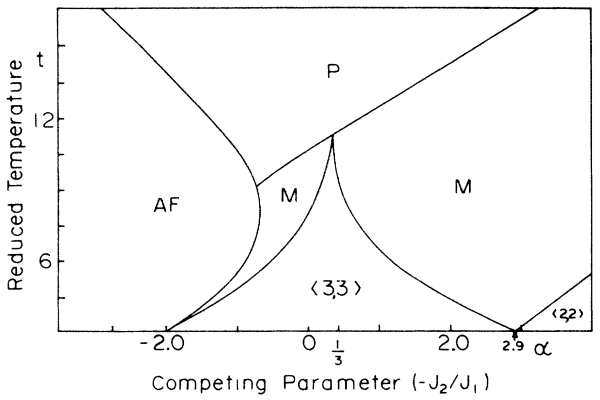

FIG. 8. Phase diagram in the (α,t) plane for $q=2$ and $\delta=1.1$.

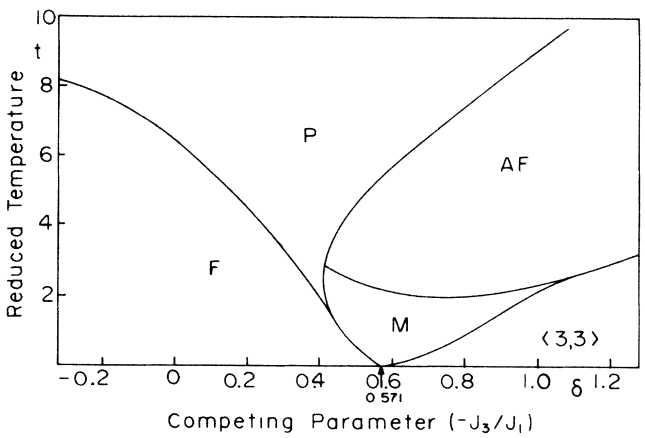

FIG. 10. Phase diagram in the (δ,t) plane for $q=2$ and $\alpha=-1.0$.

istence between the F and the AF phases as shown in Fig. 9. We note the reentrance of the AF phase into the F phase and that the point $T=0, \alpha=1$ is independent of α. For $-q<\alpha<1/(q+1)$ the phase diagram is shown in Fig. 10. We note the appearance of the modulated phase and the antiphase $\langle 3,3\rangle$ meeting with ferromagnetic and paramagnetic phases at a multicritical point at $T=0$. For

$$1/(1+q)<\alpha<(1+q)/(1+q^2)$$

the phase diagram is shown in Fig. 11. In this case the antiferromagnetic phase is absent, but we note the appearance of antiphase $\langle 2,2\rangle$ dividing the modulated phase in two regions. For $\alpha>(1+q)/(1+q^2)$ we get the phase diagram as shown in Fig. 12.

As we have pointed out in the beginning of this section the phase diagrams shown in Figs. 5–12 are obtained in a qualitatively numerical way. If we want to look at the topological structure of the modulated phases in each diagram we have to study the Vannimenus wave vector defined by $k=\lim_{N\to\infty}[n(N)/2N]$, where $n(N)$ is the number of times the local magnetization changes sign as a function of the temperature (with fixed α and δ). To go further into details of the nature of the attractors characterizing the long period commensurate or incommensurate phases we have to consider the Lyapunov exponent associated with the trajectory of the system.[2] We believed that the present model for finite q shows the same features as presented by the Vannimenus model, that is, the Lyapunov exponent is never positive meaning that the system does not exhibit strange attractors with fractal character, associated with possible chaotic phase. The same behavior has been also found for the extended Vannimenus model.[4]

The ground-state phase diagram line (α,δ) plane can be obtained analytically by minimizing the ground state energy of the F, AF, $\langle 2,1\rangle$, $\langle 2,2\rangle$, and $\langle 3,3\rangle$ phases. In Fig. 13 we show the ground-state phase diagram for the $q=2$ connectivity tree. The critical lines for an arbitrary q are given in the Table II. The phase diagrams for the case $J_1<0$ (antiferromagnetic coupling) can be obtained directly from the $J_1>0$ diagrams, since there is an iso-

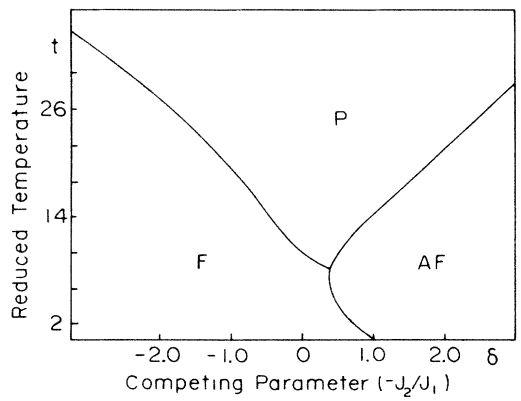

FIG. 9. Phase diagram in the (δ,t) plane for $q=2$ and $\alpha=-2.1$.

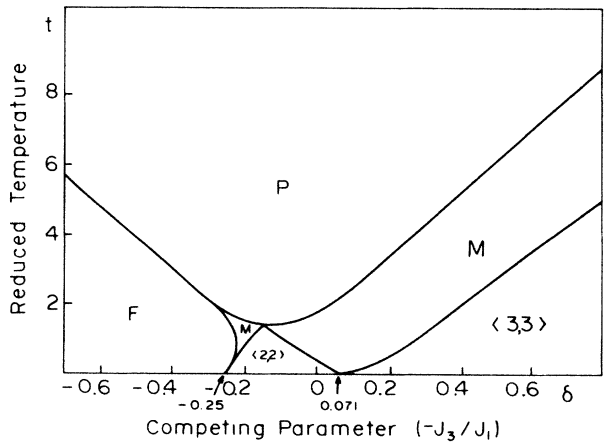

FIG. 11. Phase diagram in the (δ,t) plane for $q=2$ and $\alpha=0.5$.

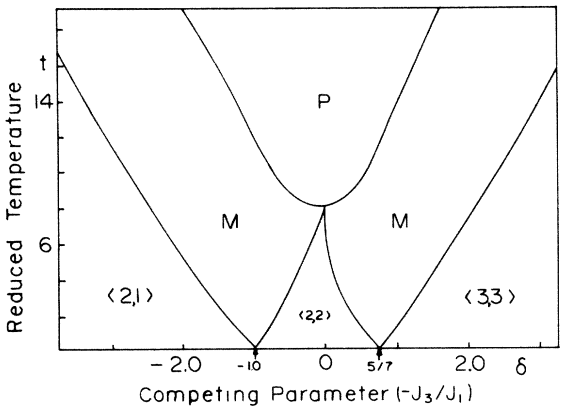

FIG. 12. Phase diagram in the (δ,t) plane for $q=2$ and $\alpha=2.0$.

morphism between the system characterized by (J_1,J_2,J_3) and that characterized by $(-J_1,J_2,J_3)$, as shown in Table III.

IV. THE INFINITE CONNECTIVITY LIMIT: $q\to\infty$

In this section we study the infinite connectivity limit $q\to\infty$ of the present model. We recover the previous results obtained by Moreira and Salinas.[14]

In order to evaluate the $q\to\infty$ limit we have to renormalize the exchange interactions coupling constants J_1, J_2, and J_3 with respect to connectivity number. This can be done by assuming that $J_1=\tilde{J}_1/q$, $J_2=\tilde{J}_2/q^2$, and $J_3=\tilde{J}_3/q^3$. To perform the $q\to\infty$ limit for the local magnetization we have to calculate, beforehand, the effective field recursion equations in the $q\to\infty$ limit. We note firstly, from Eqs. (2.8), that

$$a_{n+1}-C_{n+1}=\frac{2}{q^2}\tilde{K}_2+q[B_3^+(a_n,b_n)-B_3^-(a_n,b_n)]$$

$$=\frac{2}{q^2}\tilde{K}_2+q[A_3(a_n)-A_3(b_n)]\ , \tag{4.1}$$

TABLE II. Ground-state critical line equations in the (α,δ) plane.

Critical line	Equation
$F-AF$	$\delta=1$
$F-\langle 3,3\rangle$	$(q+1)\alpha=1-\delta(1+q+q^2)$
$F-\langle 2,2\rangle$	$(q+1)\alpha=1-\delta q$
$F-\langle 2,1\rangle$	$(q^2+1)\alpha=q+1$
$\langle 2,2\rangle-\langle 3,3\rangle$	$(q+1)\alpha=1+\delta(1+q+q^2)$
$\langle 2,2\rangle-\langle 2,1\rangle$	$(q+1)\alpha=-1-\delta(1+q+q^2)$
$\langle AF\rangle-\langle 3,3\rangle$	$\alpha+q=0$

$$b_{n+1}-d_{n+1}=\frac{2}{q^2}\tilde{K}_2+q[A_3(c_n)-A_3(d_n)]\ . \tag{4.2}$$

On the other hand

$$a_{n+1}-b_{n+1}=\frac{2}{q}\tilde{K}_1+q^2[A_3(b_{n-1})-A_3(d_{n-1})]$$

$$+q[B_3^+(a_n,b_n)-B_3^+(c_n,d_n)]\ , \tag{4.3}$$

$$c_{n+1}-d_{n+1}=\frac{2}{q}\tilde{K}_1+q^2[A_3(b_{n-1})-A_3(d_{n-1})]$$

$$+q[B_3^-(a_n,b_n)-B_3^-(c_n,d_n)]\ . \tag{4.4}$$

If we expand the equations up to the first order in $1/q$ we get

$$a_{n+1}\simeq c_{n+1}\simeq d_{n+1}+\frac{2}{q}\tilde{K}_1\ , \tag{4.5}$$

$$b_{n+1}\simeq d_{n+1}\ , \tag{4.6}$$

where

$$d_{n+1}\simeq B+\frac{1}{q}(\tilde{K}_1\tanh d_n+\tilde{K}_2\tanh d_{n-1}+\tilde{K}_3\tanh d_{n-2})\ . \tag{4.7}$$

The local magnetization can be evaluated straightforwardly by using Eqs. (4.5)–(4.7), (2.15), and (2.16), that is

$$\frac{Z_{n+1}^+}{Z_{n+1}^-}=\exp\left|2B-2\tilde{K}_1-2\tilde{K}_2+2q^3A_3(dn)+q^2\ln\left[\frac{e^{2b_{n+1}}+1}{e^{2d_{n+1}}+1}\right]+q\ln\left[\frac{e^{2a_{n+2}}+1}{e^{dn+2}+1}\right]\right|$$

$$=\exp(2B+2\tilde{K}_1\tanh d_{n+1}+2\tilde{K}_2\tanh d_{n+2}+2\tilde{K}_3\tanh d_n) \tag{4.8}$$

$$=\exp(2d_{n+3})\ . \tag{4.9}$$

Therefore $\langle\sigma_{n+1}\rangle=\tanh d_{n+3}$, and if we use Eq. (4.7) we can finally get the recursion relation for the local magnetization in the $q\to\infty$ limit, that is

$$\langle\sigma_{n+1}\rangle=\tanh\left[B+\frac{1}{\tilde{t}}(\langle\sigma_{n-1}\rangle-\tilde{\alpha}\langle\sigma_{n-2}\rangle-\tilde{\delta}\langle\sigma_{n-3}\rangle)\right]\ , \tag{4.10}$$

where $\tilde{t}=K_BT/\tilde{J}_1$, $\tilde{\alpha}=-\tilde{J}_2/\tilde{J}_1$, and $\tilde{\delta}=-\tilde{J}_3/\tilde{J}_1$.

The phase diagram in the $(\tilde{\alpha},\tilde{t})$ plane for several values of $\tilde{\delta}$ for the present $q\to\infty$ limit model has been already studied in Ref. 14. Nevertheless, the ground state phase diagram in the $(\tilde{\alpha},\tilde{\delta})$ plane can be obtained directly from the $q\to\infty$ limit of the critical lines, given in Table II, as we show in Table IV. The ground state phase diagram $(\tilde{\alpha},\tilde{\delta})$ is shown in Fig. 14. We note that the antiferromag-

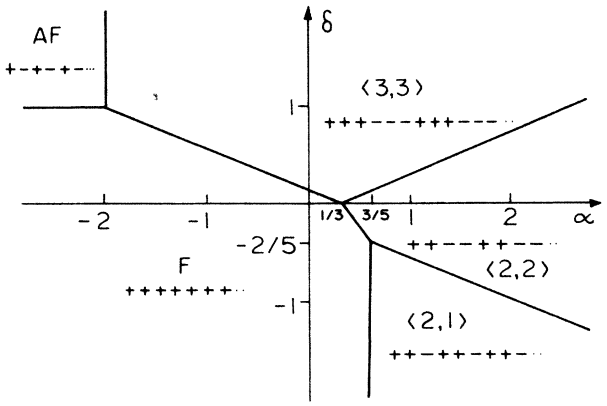

FIG. 13. Ground-state phase diagram in the (α,δ) plane for $q=2$.

netic ground-state is not stable in the $q\to\infty$ limit, while the antiphase $\langle 2,1\rangle$ is.

V. CONCLUSIONS

We have solved exactly the Ising model on the Bethe lattice with arbitrary coordination number q and with competing interactions between first-, second-, and third-nearest-neighbor spins belonging to the same branch (consecutive generations) and under an external field. Interactions between sites belonging to the same generations are excluded from the present model. The partition function, the local magnetization, and the pair correlation function are calculated exactly by solving, numerically, the coupled set of the recursion equations of appropriated effective fields. These effective fields are defined by the ratio of the partition functions of pruned branches of the lattice. The particular choice of these branches in our approach is an essential feature for calculating the pair correlation function. The partition function is expressed by means of the partial partition function of these branches, and can also be obtained numerically by evaluating the fixed points or attractors of the effective field recursion relations.

The phase diagrams in the space (t,α,δ), where t is the reduced temperature and α and δ are the competing parameters, are obtained by observing the changes in the behavior of the fixed points (or attractors). The phases are identified by the local magnetization and the pair correlation functions. Each phase is characterized by a particular sequence of fixed points. Besides the paramagnetic and the ferromagnetic phases, there are a large (infinite) number of commensurate phases. The main commensurate phases, namely the antiphases $\langle 2,2\rangle$, $\langle 3,3\rangle$, $\langle 2,1\rangle$, and $\langle 1,1\rangle$ are stable even at $T=0$, as shown in Fig. 11, for the $q=2$ case. We have shown several phase diagrams for different ranges of values of the competing parameters α and δ. The antiphases $\langle 3,3\rangle$, $\langle 2,1\rangle$, and $\langle 1,1\rangle$ are characteristic of the present model since they arise from the frustration effects introduced by the third-nearest-neighbor competing interactions. We were not able to give the boundaries between the higher commensurate phases in the modulated region of the phase diagrams due to our lack of computational facilities to handle a set of high-order coupled recursion relations. However, we note the existence of a multiphase point at finite temperature for the particular range of values $0<-\delta<2/(1+q^2)$ as shown in Fig. 5. For $\delta=0$ we recover the Vannimenus phase diagram[2] where the multiphase point is located at $T=0$ and $\alpha=1/(1+q)$. for $\delta>0$ $(J_3<0, J_1>0)$ we note the appearance of the antiphase $\langle 3,3\rangle$ centered about the point $T=0, \alpha=1/(1+q)$, and dividing the modulated phase in two regions (see Fig. 7). For $\delta>1$ the antiphase $\langle 1,1\rangle$ (truly antiferromagnetic phase) is stable against the

TABLE III. Isomorphism between the phase diagram of the (J_1,J_2,J_3) and the $(-J_1,J_2,J_3)$ systems.

$J_1>0$	$J_1<0$
(F) ↑↑↑↑↑↑↑	(AF) ↑↓↑↓↑↓↑↓
(AF) ↑↓↑↓↑↓↑	(F) ↑↑↑↑↑↑↑↑
$\langle 2,1\rangle$ ↑↑↓↑↑↓↑	$\langle 3,3\rangle$ ↑↑↑↓↓↓↑↑↑
$\langle 2,2\rangle$ ↑↑↓↓↑↑↓↓	$\langle 2,2\rangle$ ↑↑↓↓↑↑↓↓
$\langle 3,3\rangle$ ↑↑↑↓↓↓↑↑↑	$\langle 2,1\rangle$ ↑↑↓↑↑↓↑↓

TABLE IV. Ground-state critical line equation in the $q\to\infty$ limit.

Critical line	Equation
$F-AF$	$\tilde{\delta}=\infty$
$F-\langle 3,3\rangle$	$\tilde{\delta}=1-\tilde{\alpha}$
$F-\langle 2,2\rangle$	$\tilde{\alpha}=1$
$F-\langle 2,1\rangle$	$\tilde{\alpha}=1$
$\langle 2,2\rangle-\langle 3,3\rangle$	$\tilde{\delta}=\tilde{\alpha}-1$
$\langle 2,2\rangle-\langle 2,1\rangle$	$\tilde{\delta}=-(1+\tilde{\alpha})$
$AF-\langle 3,3\rangle$	$\tilde{\alpha}=-\infty$

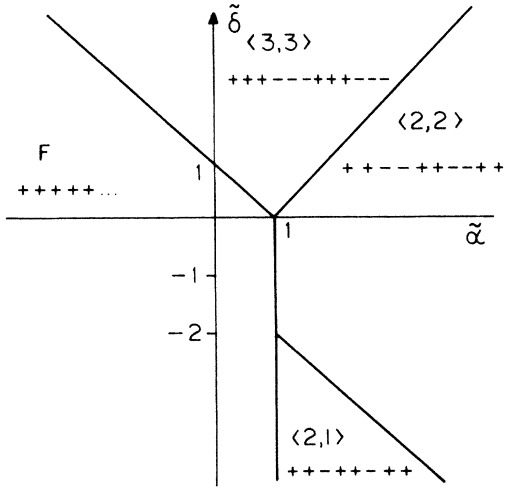

FIG. 14. Ground-state phase diagram in the (α,δ) plane for $q=\infty$.

ferromagnetic phase and has a reentrant character over the whole diagram, as shown in Fig. 8. In this region the multiphase point $t=0, \alpha=-q$ is independent of δ. The phase diagram is also studied in the plane (t,δ) for four ranges of values of α showing similar features, as can be seen in the Figs. 9–12. The ground-state phase diagrams are obtained analytically for general q by minimizing the energy of the F, AF, $\langle 2,1\rangle$, $\langle 2,2\rangle$, and $\langle 3,3\rangle$ phase at $T=0$, as shown in Table II and in Fig. 13. For $q=1$ we recover the result of Barreto and Yeomans[11] for the A3NNI model in the cubic lattice.

Finally we worked out the $q\to\infty$ limit recovering the previous results of Moreira and Salinas[14] where the set of high-order coupled recursion relations reduces to a single third-order recursion relation for the effective magnetization. We note that in the $q\to\infty$ limit the antiferromagnetic phase is no longer stable at $T=0$ while the antiphase $\langle 2,1\rangle$ remain stable. The ground-state critical lines in the $q\to\infty$ limit are shown in Table IV and in Fig. 14.

---

*Permanent address: Departamento de Física, Universidade Federal de Alagoas 57000, Maceió, Alagoas, Brazil.

[1]For a review see R. J. Baxter, *Exactly Solved Models in Statistical Mechanics* (Academic, New York, 1982).

[2]J. Vannimenus, Z. Phys. B **43**, 141 (1981).

[3]S. Inawashiro and C. J. Thompon, Phys. Lett. **97A**, 245 (1983).

[4]S. Inawashiro, C. J. Thompson, and G. Honda, J. Stat. Phys. **33**, 419 (1983).

[5]T. Horiguchi and T. Morita, J. Phys. A **16**, 3611 (1983); J. Stat. Phys. **35**, 355 (1984).

[6]A. M. Mariz, C. Tsallis, and E. L. Albuquerque, J. Stat. Phys. **40**, 577 (1985).

[7]C. S. Yokoi, M. J. de Oliveira, and S. R. Salinas, Phys. Rev. Lett. **54**, 163 (1985).

[8]T. Morita, Phys. Lett. **94A**, 232 (1983).

[9]Y. Yamada and N. Hamaya, J. Phys. Soc. Jpn. **52**, 3466 (1983).

[10]W. Selke, M. Barreto, and J. Yeomans, J. Phys. C **18**, L393 (1985).

[11]M. Barreto and J. Yeomans, Physica (Utrecht) **134A**, 84 (1985).

[12]J. Randa, Phys. Rev. B **32**, 413 (1985).

[13]C. J. Thompson, J. Stat. Phys. **27**, 441 (1982).

[14]J. G. M. A. Moreira and S. R. Salinas, J. Phys. A (to be published).

[15]Equation (2.18) is the same as equation (2.13) of Ref. 13.

[16]F. Peruggi, J. Phys. A **16**, L713 (1983).

[17]The higher-order commensurate and incommensurate phases have to be distinguished within the precision of the numerical calculation.